AD-A119 080 NAVAL RESEARCH LAB WASHINGTON DC F/G 20/5
LASER-ABLATIVE ACCELERATION OF TARGETS TO NEAR INERTIAL FUSION --ETC(U)
AUG 82 B H RIPIN, S E BODNER, P G BURKHALTER
UNCLASSIFIED NRL-MR-4916 NL

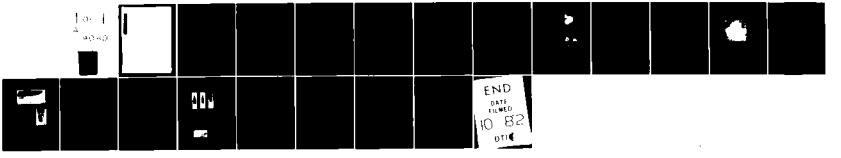

END
DATE FILMED
10 82
DTIC

SECURITY CLASSIFICATION OF THIS PAGE (When Data Entered)

REPORT DOCUMENTATION PAGE		READ INSTRUCTIONS BEFORE COMPLETING FORM
1. REPORT NUMBER NRL Memorandum Report 4916	2. GOVT ACCESSION NO. AD-A119 080	3. RECIPIENT'S CATALOG NUMBER
4. TITLE (and Subtitle) LASER-ABLATIVE ACCELERATION OF TARGETS TO NEAR INERTIAL FUSION CONDITIONS		5. TYPE OF REPORT & PERIOD COVERED Interim report on a continuing NRL problem. 6. PERFORMING ORG. REPORT NUMBER
7. AUTHOR(s) B.H. Ripin, S.E. Bodner, P.G. Burkhalter, H. Griem*, J. Grun**, H. Hellfeld, M.J. Herbst, R.H. Lehmberg, C.K. Manka†, E.A. McLean, S.P. Obenschain, J.A. Stamper, R.R. Whitlock, and F.C. Young		8. CONTRACT OR GRANT NUMBER(s)
9. PERFORMING ORGANIZATION NAME AND ADDRESS Naval Research Laboratory Washington, DC 20375		10. PROGRAM ELEMENT, PROJECT, TASK AREA & WORK UNIT NUMBERS DOE AI08-79DP 40092 (172) 47-0859-0-2
11. CONTROLLING OFFICE NAME AND ADDRESS Department of Energy Washington, DC 20545		12. REPORT DATE August 30, 1982 13. NUMBER OF PAGES 19
14. MONITORING AGENCY NAME & ADDRESS(if different from Controlling Office)		15. SECURITY CLASS. (of this report) UNCLASSIFIED 15a. DECLASSIFICATION/DOWNGRADING SCHEDULE

16. DISTRIBUTION STATEMENT (of this Report)

Approved for public release; distribution unlimited.

17. DISTRIBUTION STATEMENT (of the abstract entered in Block 20, if different from Report)

18. SUPPLEMENTARY NOTES

*Present address: University of Maryland, College Park, MD
**Present address: Mission Research Corporation, Alexandria, VA
†Present address: Sam Houston State University, Huntsville, TX
This work was supported by the U. S. Department of Energy

(Continues)

19. KEY WORDS (Continue on reverse side if necessary and identify by block number)

Laser-fusion
Laser-plasma interactions
Plasma
Fusion

20. ABSTRACT (Continue on reverse side if necessary and identify by block number)

NRL is investigating the physics issues involved in the direct illumination approach to laser fusion. Millimeter diameter planar targets are ablatively accelerated to speeds and conditions near those required of fusion pellet shells using 3-5 ns, 1.05 μm light from the PHAROS II laser. At 5×10^{13} W/cm^2 targets were accelerated to 160 km/sec with a velocity uniformity of $\pm 7\%$ through twenty times the initial target thickness and while remaining cool (< 10 eV). A joint NRL-LLNL experiment on SHIVA extended these results to beyond 10^{14} W/cm^2; the uniformity of acceleration of dense

(Continues)

DD FORM 1 JAN 73 1473 EDITION OF 1 NOV 65 IS OBSOLETE
S/N 0102-014-6601

SECURITY CLASSIFICATION OF THIS PAGE (When Data Entered)

18. Supplementary Notes (Continued)

9th International Conference on Plasma Physics and Controlled Nuclear Fusion Research
Baltimore, MD USA 1 — 8 September 1982
Paper IAEA-CN-41/B-3

20. Abstract (Continued)

mm-diameter targets improved to better than ± 3.5% and the interaction physics remained benign. Also, absorption was above 65% and fast electrons were a minor energy channel. Thus, the moderate-irradiance direct-illumination approach appears to be an attractive option for laser fusion. To further verify this conjecture, particular attention is paid to the factors affecting the uniformity of acceleration or targets such as laser beam and target uniformity requirements, and various hydrodynamic mechanisms such as Rayleigh-Taylor and Kelvin-Helmholtz instabilities. The study of the behavior of laser-plasma interactions is also extended into regimes closer to those expected to be encountered in reactor sized pellets. Large plasmas with long scalelengths are generated using two-pulse methods; backscatter, fast electron production, etc. are observed as the laser intensity is increased beyond 10^{14} W/cm^2. New diagnostic techniques are also discussed for measurements of plasma properties. These include: double-foil methods, x-ray backlighting, tracer-material techniques, Zeeman splitting measurements of magnetic fields, and others.

CONTENTS

INTRODUCTION 1

DESCRIPTION OF EXPERIMENT 1

INTERACTION PHYSICS 2

HIGH SPEED UNIFORM TARGET ACCELERATION 3

A. Nonuniformities 5
B. Beam nonuniformities and smoothing 5
C. Preheat 8
D. Target nonuniformities 11

CONCLUSIONS AND SUMMARY 13

REFERENCES 15

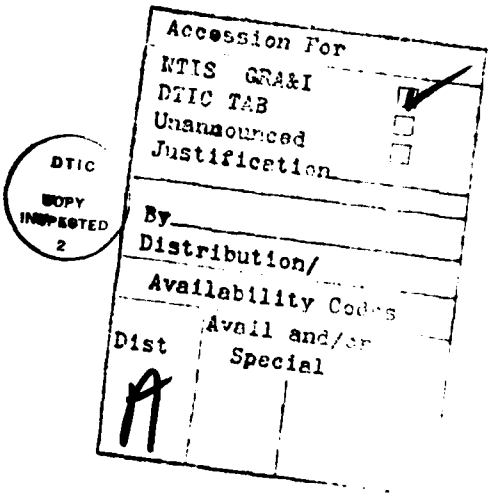

LASER-ABLATIVE ACCELERATION OF TARGETS TO NEAR INERTIAL FUSION CONDITIONS

INTRODUCTION

NRL is investigating the acceleration of dense material to high velocity by the direct-illumination of targets with laser light; specifically we are addressing the four most critical interaction physics issues for laser fusion viability, i.e., coupling efficiency, ablation pressure, fuel isentrope and target acceleration uniformity.[1-12] It is hypothesized that a suitable laser irradiance window for 1-μm laser light exists in the low-10^{14} W/cm^2 range. We employ planar targets in our experiments since planar geometry affords diagnostic advantages over pellets in observations of what would be the pellet inner wall and, for a given laser energy, can access longer plasma scalelengths. Also, many results can be transferred to spherical geometry. However, neither spherical convergence nor ignition effects can be addressed.

DESCRIPTION OF EXPERIMENT

The NRL PHAROS II Nd-phosphate laser ($\lambda \approx 1.05$ μm) has two beams which are usually combined using a polarizer into one beam for target experiments.[13] Each laser beam outputs up to 500 J in 3-4 ns pulses; experiments are usually performed by focusing the light to millimeter diameters onto thin planar targets placed in the quasi-near field of the f/6 aspheric focusing lens. The intensity is uniform across the focal spot to $\pm$ 30%, unless intentionally structured; the focal distribution and pulse temporal history are monitored on every shot. Sometimes only one beam of the laser is used to accelerate the target, with the typical 3-4 ns multihundred joule pulse, while the other beam delivers about 50J in a short pulse duration (< 500 ps). The short duration beam is used to generate x rays for x-ray backlighting or directly for interaction studies in large scalelength plasmas. In addition, a short duration laser probe pulse, also chopped out of the main oscillator pulse, is used for optical shadowgraphy, interferometry and scattering diagnostics.

The basic experimental arrangement has been described extensively elsewhere.[2-12] Standard diagnostics, also described previously, monitor the scattered laser light, absorbed plasma energy, velocity and momentum, x-ray emission spectra, underdense plasma density, and accelerated target temperature. X-ray backlighting images the dense portions of the accelerating target and the double-foil method is able to measure velocity nonuniformities down to about the 1% level. The tracer dot technique, to be described further, enables fluid flow visualization, improved spectroscopic methods, and even velocity gradient determinations. Zeeman splitting of CV ultraviolet spectral lines provides self-generated magnetic field information.

Manuscript submitted August 16, 1982.

INTERACTION PHYSICS

The interaction physics of 3 to 4 nanosecond 1-μm laser pulses for laser intensities below 10^{14} W/cm^2 has favorable properties for accelerating material.[2,4] The laser light absorption, η_a, is high, typically 70-80%, and the energy is deposited in a thermal electron distribution of 300-400 eV. Also, fast electron population and stimulated Brillouin backscatter are found to be negligible under these conditions. Ablation pressure, $P = \dot{m}\, u$, scales with the 0.8 power of absorbed irradiance ($P = 10$ Mbar at $I_a = 5 \times 10^{13}$ W/cm^2); likewise the mass ablation rate, $\dot{m}$, and the ablation velocity, u, scale with 0.6 and 0.2 powers of I_a respectively.[6,7] Hydrodynamic efficiency, η_h, defined as the kinetic energy of the target divided by the absorbed energy, as high as 20% was obtained, resulting in overall coupling efficiencies $\eta_a\, \eta_h$ up to 16%. The pulse duration is long enough to establish approximately steady-state ablation and the irradiated areas are deliberately large (1 mm^2) and uniform to avoid the influence of edge effects.[2,3,6,7] The fluid flow of the ablating plasma, mapped out by using a unique tracer method,[14,15] is seen to be approximately one-dimensional and laminar in the ablating plasma acceleration region near the target.

When 1-μm laser intensities approach 10^{14} W/cm^2 the laser-plasma coupling begins to exhibit signs of detrimental high-irradiance effects such as increased backscatter, fast electron and ion production, self-generated magnetic fields, and so on. To address these issues, especially under conditions approaching the long (mm's) density scalelengths of reactor pellets, we have undertaken two approaches:

1. Density scalelengths of the target plasma are increased using a high energy (250 J) 3-ns pulse with a big focal spot, which creates a large (250-600 μm) plasma. The interactions of a second, short-duration (< 500 psec) and delayed pulse, which is focused to high intensity into the large expanding plasma is observed. Initial results of this study show increased direct backscatter over that seen at lower irradiances although the maximum backscatter through the focusing lens has not exceeded 10% for irradiances up to mid-10^{14} W/cm^2,[16] A surprising result is a concomitant decrease of both high energy x-ray emission (fast electrons) and second harmonic emissions in the large plasma case. Possible explanations for this behavior include reduced resonance absorption in the larger density scalelengths, or reduced light intensity reaching the critical surface due to increased inverse Bremsstrahlung absorption or increased Brillouin scatter.

2. Multi-kilojoule, 3-ns single-pulse experiments with large focal spots (1-mm) above 10^{14} W/cm^2 were performed jointly by NRL and LLNL on the SHIVA laser. The large spot size and energy creates large (600 μm) underdense plasma. In this regime the absorption decreased to about 65% but the scattered

light appeared uniformly distributed over 2π-sr. Three-halves-ω harmonic light was observed at about the 1% level but no signature of Raman scattering was seen. Moreover, the hot electron fraction increased to about 3% of the absorbed energy. A two-plasmon decay instability may be occurring here.[18]

In both cases described above, changes were seen in the interaction physics above 10^{14} W/cm^2 in the presence of large plasmas which are undesirable for the laser fusion application. Although the magnitude of these effects was small enough not to impact a reactor pellet performance, the physics involved is obviously poorly understood and, therefore, more investigations of still larger plasmas are needed to extrapolate to reactor-like conditions.

Several recent advances in diagnostics have enabled us to characterize the underdense interaction plasma more completely.

Small localized tracer materials embedded in the target surface, such as illustrated in Figure 1, are collisionally confined by, and flow out with, the blowoff plasma.[14-16] When the spectral emission of the tracer material is imaged the flow properties of the plasma fluid are visualized. When the diameter of the tracer material flow-tube is correlated with an independent plasma density measurement, such as interferometry, then flow velocity gradients are obtained; these are the first such measurements of the velocity profile (which causes an important uncertainty in Brillouin backscatter calculations). Finally, plasma spectroscopy is significantly improved by using tracers as the spectroscopic source since source broadening, opacity effects, and the need to correct for observation along a plasma chord are greatly reduced. An example of improved spectral resolution with tracers is shown in Fig. 1. Complete density and temperature profiles from the overdense region (2 x 10^{21}/cc) into the very underdense region are obtained.

A special technique used to measure self-generated magnetic fields in the underdense plasma is from Zeeman splitting of the 2271-2278 Å CV lines.[19] Time-resolved observations were made of the line emission in each of two polarizations and corrections for opacity effects, Doppler shifts, instrumental and Stark broadening were incorporated; a 300 kG upper limit on the magnetic field was established 8 ns after the peak of the laser pulse.

HIGH SPEED UNIFORM TARGET ACCELERATION

Reasonably uniform, high-speed target accelerations have been achieved in the ablation regime described above; for example; at 3 x 10^{13} W/cm^2 CH targets were accelerated to 160 km/sec with better than $\pm$ 7% velocity uniformity.[9,20] The double-foil diagnostic is used to determine the target speed and uniformity; this technique is discussed here and elsewhere.[6,7,9,11,12,20] The velocity uniformity of the accelerated target represents a net smoothing of the $\pm$ 30% nonuniformities in the incident focal

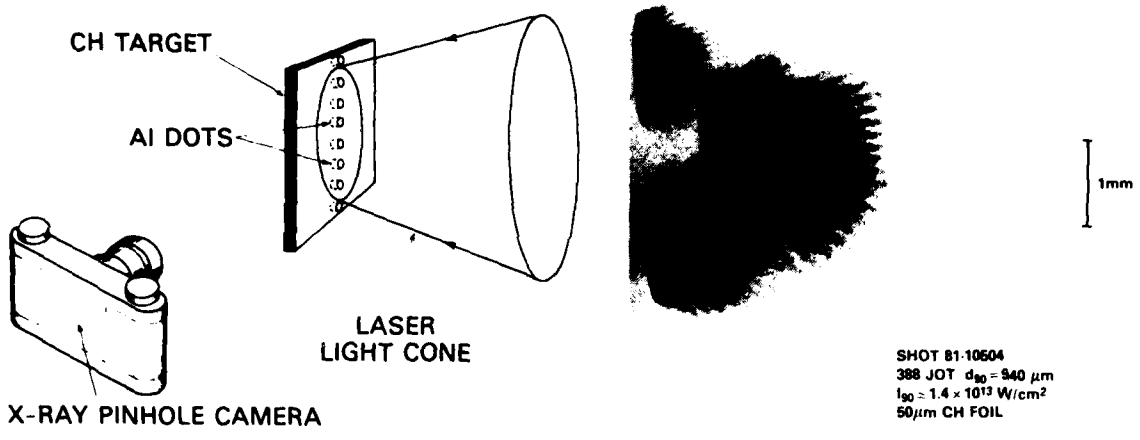

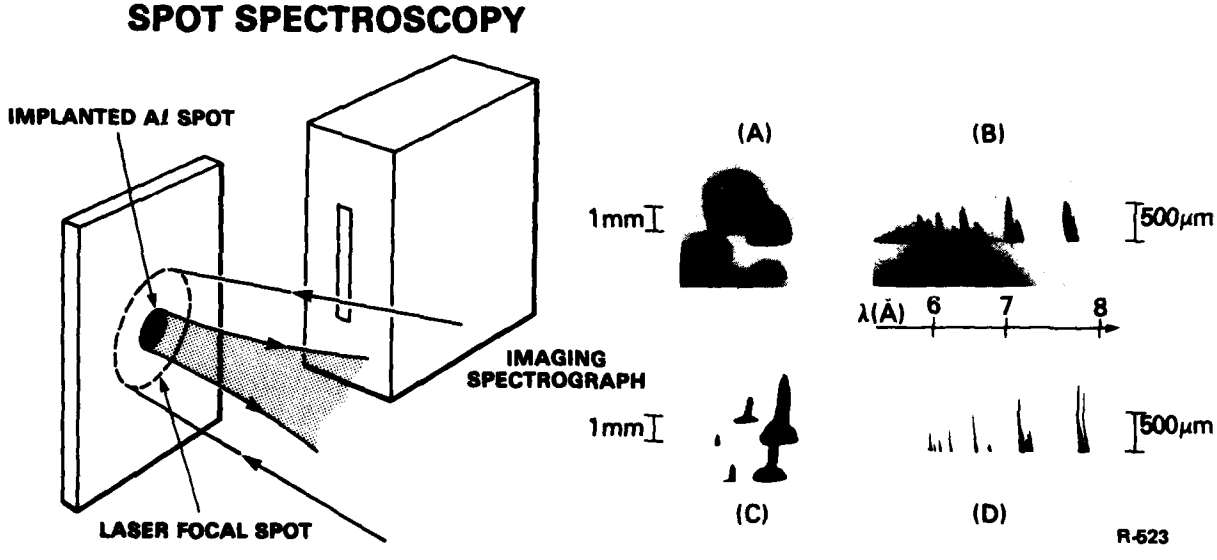

Fig. 1 — Tracer material diagnostic technique. A schematic of the experimental arrangement is shown in the upper left; small Al dots are implanted in a low-Z (CH) target; the enhanced x-ray emission from the Al tracer plasma is visualized by a filtered pinhole camera. The upper right shows a set of 4 pinhole camera images showing the tracer flow visualization. Use of the tracer technique for spectroscopic measurements is shown in the lower left and an example of the improved spectral resolution possible is shown in lower right. The data compares the x-ray pinhole photo and spectra for a solid Al target (A) and (B) with an Al tracer dot shot in (C) and (D).

region by a factor of 4. The rear surface temperature of the target throughout the acceleration phase ($t < +2$ nsec) under the same conditions is below 7 eV; the temperature then peaks at 10 eV after the acceleration phase. These results approach the velocity, uniformity and preheat requirements of a high-gain pellet shell. At 10^{14} W/cm^2 the ablation pressure and velocity uniformity of the accelerated targets improved further.[17]

A. Nonuniformities

For most purposes the accelerated target must have a very uniform velocity across its diameter; in fact, uniformities of the order of 1% may be needed to achieve the high pellet compressions required to give high gain performance. Many mechanisms can degrade target acceleration uniformity. Kinematic mechanisms are manifestations of a nonuniform pressure or mass; these include nonuniformities in the incident beam which reach the ablation surface (for which $\delta v \propto \delta P$) and accentuated versions in targets which are thinning locally due to an intensity dependent mass ablation rate. Care must be taken not to mistake the latter effect for hydrodynamic instability since both effects cause velocity variations which increase more rapidly than linearly in time. Target areal density variations will also cause a kinematic nonuniformity, or worse. Incident beam nonuniformities can be accentuated by macroscopic refraction, self-focusing, filamentation,[21] jetting[10,15] and magnetic fields,[19,22] in the underdense plasma. Also, as previously mentioned, nonuniform heating of the target interior can cause local blistering. All these effects can potentially seed or enhance hydrodynamic instability. Conditions that permit growth of hydrodynamic modes may occur at several stages in the target acceleration-deceleration history. Rayleigh-Taylor and Kelvin-Helmholtz modes may occur wherever a light fluid is accelerating into a denser fluid; Benard convection cells may develop in response to an inverted temperature gradient. In addition to preventing a high density final state, hydrodynamic instability can cause various layers in the target to mix and degrade the performance.

B. Beam nonuniformities and smoothing

Nonuniformities of accelerated targets can be observed using: optical backlighting,[2] doppler reflectrometry,[8,23] double-target collisions,[11] and x-ray backlighting.[24] The latter two are emphasized here because they are sensitive to the high density (or momentum carrying) portion of the target and they are capable of discerning the small nonuniformities (few %) allowed.

In the double-target method,[11,6-9] the collision of the accelerated target with a displaced diagnostic foil is observed with a streak camera which time-resolves the visible light emission, caused by impact, across a diameter of the impacted foil rear surface. Nonuniformities in the target velocity profile are easily seen as time delays of the emission and observation of perturbations as small as 1% are feasible.[20]

The double-foil method has demonstrated the following features of targets accelerated with artificially introduced laser beam nonuniformities:

- o Target velocity nonuniformities are substantially reduced over those of the applied laser beam intensity, and,
- o Target velocity variations diminish with both increasing irradiance and decreasing perturbation scalelength.

For example, structure in the incident beam with a peak-to-valley distance of 140 μm ($\Lambda \simeq 280$ μm) and 6:1 amplitude ratio result in only $\pm$ 10% target velocity variations at an average irradiance of 10^{13} W/cm^2.

X-radiographs of accelerated targets, such as the one shown in Figure 2, show the high-density ($\rho > 0.03\ \rho_{solid}$) regions of the target intact, to be well-localized (40 μm) in space. and an acceleration uniformity in agreement with results of the double-foil method.[24] The target is seen to be intact and localized even though the x-radiogram was taken at a time (+ 5 nsec) well after the end of the acceleration phase (the laser pulse is effectively over at +2 nsec) where target decompression and disassembly can expand the target. Further measurements must be made to resolve the peak target densities and thicknesses beyond the limits already given. X-radiographs of accelerated targets in the double-target mode exhibit nonuniformities which corroborate the corresponding double-target inferences.

The observed smoothing of the target velocity profile, relative to that of the incident beam, is due to the thermal heat diffusion between the absorption region, where the energy is deposited, and the ablation surface, where the bulk of the pressure is applied to the target. This "cloudy day" effect most effectively washes out hot spots when the distance d between absorption and ablation exceeds the perturbation scalelength Λ. Additional evidence that lateral thermal conduction can more effectively wash out beam nonuniformities at increasing irradiance is seen when the flow lines are mapped out in the ablating plasma by the enhanced x-ray emission of a linear array of Al dots implanted in the plastic target.[15,20] Classical thermal transport in this region appears adequate to explain our present data for $I \lesssim 10^{14}$ W/cm^2. This inference is based on the agreement of hydrodynamic codes, assuming classical thermal conduction, with such experimental results as: target accelerations, ablation pressures and velocities,[6] and predictions of d which adequately explain the uniformity data.[20,25-27] The smoothing length d increases with laser irradiance and wavelength like $I^{0.7}\ \lambda^{2.7}$ in this spherical model;[28] an analytic planar model[27] yields a similar scaling relation, i.e., $d \propto I^{4/3}\ \lambda^{4/3}$. These models

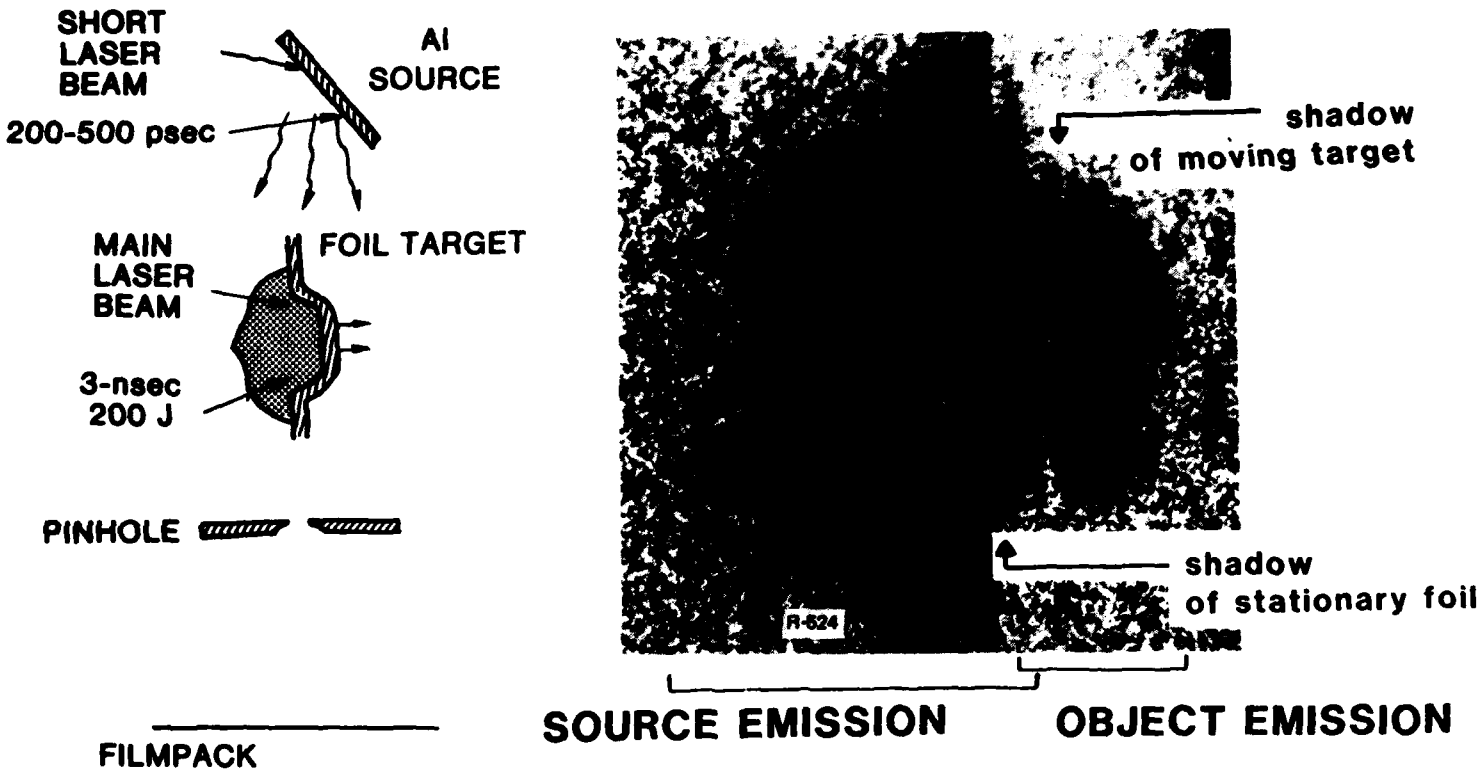

Fig. 2 — X-radiograph of an accelerated carbon foil target 5-ns after the peak of the laser pulse

adequately explain the observed enhanced smoothing with irradiance, and predict better smoothing with longer wavelength and increased irradiance.

To test whether uniformity actually improved with irradiance, experiments were done on the SHIVA facility where 3-4 kJ of 1.06 μm, 3 ns laser light was focused onto 1 mm diameter areas of planar carbon targets at 10^{14} W/cm^2 by overlapping 10 beams of the laser. Even though the light absorption fraction decreased to 65% and edge effects were evident, the ablation pressure reached 6 Mbar and, most encouragingly, the target velocity uniformity improved by more than a factor of two over the 3 x 10^{13} W/cm^2 case.[17] This is as expected from the cloudy day effect scaling. Figure 3a shows an x-ray backlighting streak photograph showing the acceleration of the target foil and subsequent impact with the second foil (impact foil). The final target velocity was above 10^7 cm/sec and clearly remained intact. The corresponding double-foil uniformity measurement from the luminosity of the impact foil, shown in Fig. 3b, demonstrates the excellent target uniformity obtained ($\lesssim \pm$ 3.5%) despite the 30% laser intensity variations thought to be placed on target. These results are summarized in Table I.

C. Preheat

Two major methods are used to measure the temperature of the target material during acceleration (preheat). Time-resolved optical pyrometry[5] monitors the optical emission from the rear of the target; this is related to temperature through blackbody emission. This technique has been used extensively for these measurements and the blackbody assumption has been verified.[5] Another method, which has been used to corroborate the pyrometry, involves measuring the free-expansion velocity of the preheated material.[29] This technique is sensitive to the internal target temperature.

For experiments done at NRL in the mid-10^{13} W/cm^2 irradiance regime and below, the major source of the observed preheating ($\lesssim$ 10 eV) is believed to result from radiant heating due to x-ray emission below a few keV coming from the several hundred electron volt plasma temperature in the interaction region.[5] The preheat level is insensitive to irradiance in this region of the spectrum. The spectral emission and absorption characteristics of the target are complex due to the presence of atomic lines. Nonetheless, a calculation of the radiant heating of aluminum targets using observed absolute x-ray spectra above 1 keV and cold material absorptivities[5] adequately explains the heating in thin Al-targets at low irradiance. Sufficiently quantitative comparisons of radiant heating with lower Z targets, e.g., CH and C, have not yet been made; however, preliminary measurements of photon flux in the 200-300 eV range can account for most of the observed heating. The role of shock wave heating in these

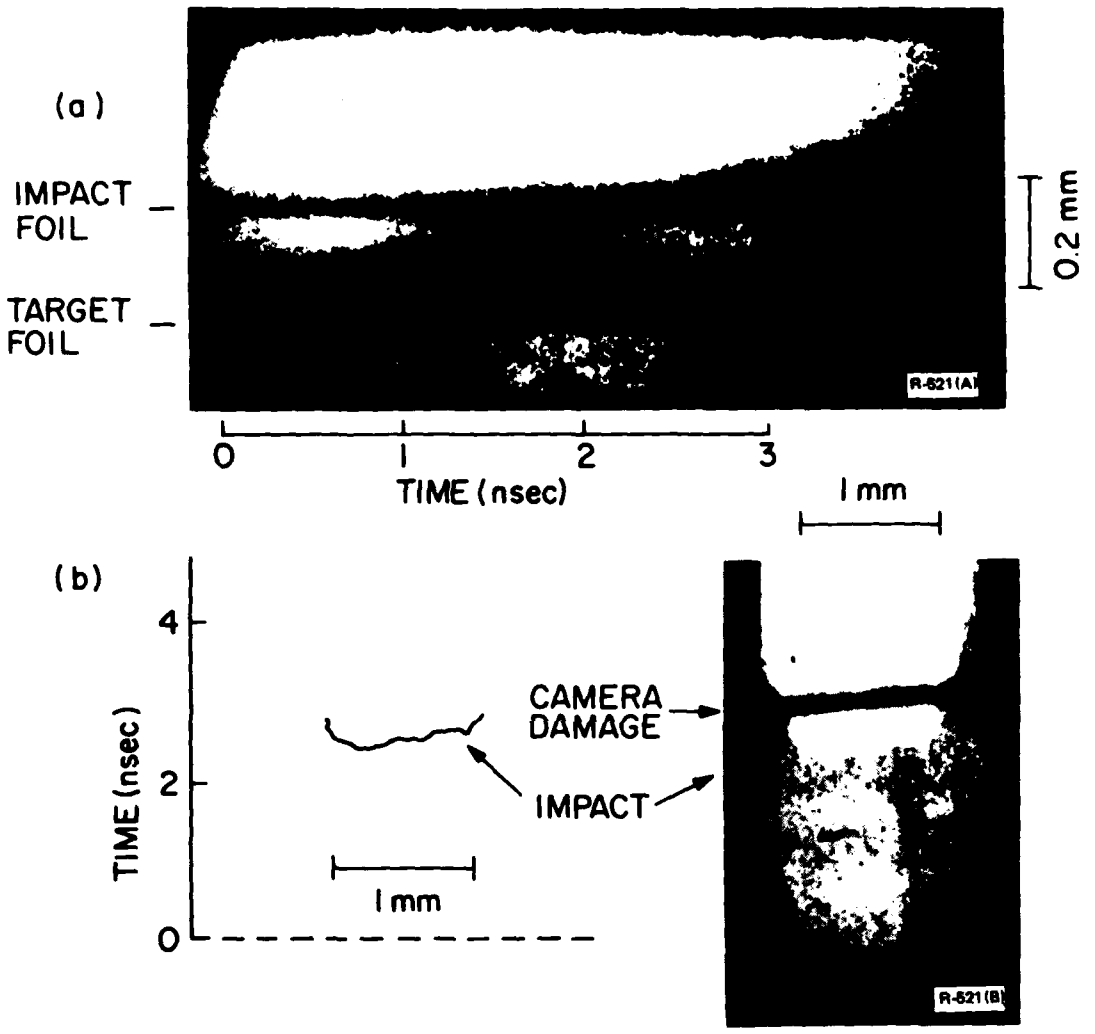

Fig. 3 — Acceleration and velocity uniformity data for a target acceleration with a 10^{14} W/cm^2, 3-4 kJ SHIVA laser pulse. A streak photograph of the x-ray backlit double-foil is seen in (a). The optical emission across the diameter of the rear of impact foil is seen in (b); the velocity uniformity inferred from these data is a 8% tilt, ± 3.5% nonuniformity across 800 μm, and < + 2.5% nonuniformity across 200 μm scalelengths.

targets is not well established. The laser pulse risetime in our experiments, $t_r \overset{\sim}{\sim} 1.7$ nsec, is generally long compared to sonic transit times through thin targets ($\sim$ 10 μm/nsec); this minimizes strong shock formation and shock induced preheat. Electron thermal conduction and radiation diffusion drive the deposited heat front towards the rear surface. For these reasons the rear surface temperature continues to rise after the laser pulse terminates. Some additional properties of the preheat are found from the dependence of peak rear surface temperatures on target areal mass density. There is little preheat dependence with either target material or irradiance, but the temperature decreases with increased target thickness. This dependence is encouraging since a thicker target should be less susceptible to x-ray preheat even with longer pulse duration.

The experiments done at 10^{14} W/cm^2 on SHIVA, however, exhibited temperatures up to 15 eV.[17] In this case the 3% 10 keV hot electron population could account for the major portion of the preheat.

Although the preheat levels observed in our target acceleration experiments are below 15 eV, it is desirable that they be further reduced for laser fusion. The thicker walls in reactor sized targets should reduce the preheat to acceptable levels. Additionally, the use of very low-Z target materials (such as lithium, hydrogen, or beryllium) to reduce the radiant heat flux, the use of longer rise-time pulses to control shock-wave formation, and the use of special target layers for x-ray and shock-wave shields are preheat-reducing measures that can be employed if needed.

Table 1 — Experimental status of ablative acceleration of dense material to high velocity

Critical Element	NRL Experiments	NRL-LLNL Expt.[17]
Coupling Efficiency (total)	0.16	
absorption	0.8	0.65 ± .1
hydrodynamic	0.2	
Ablation Pressure	3 Mbar at 3×10^{13} W/cm^2	6 Mbar at 10^{14} W/cm^2
target velocity	160 km/sec	100 km/sec
Target Isentrope	< 10 eV	$\sim$ 15 eV
Acceleration Uniformity		
δv/v	± 7%, $\Lambda \sim$ 200 μm	± 3.5%, $\Lambda \sim$ 800 μm
		< ± 2.5%, $\Lambda \sim$ 200 μm

D. Target Nonuniformities[30,31]

Nonuniformities also result from target imperfection and any resulting hydrodynamic instability. These effects are examined experimentally in a manner analogous to those used in the beam uniformity studies, i.e., with purposely structured targets and use of the double-target method to infer the resulting velocity profile across the target diameter. Several types of target perturbations may be envisioned, these include: ripples, areal density variations, thickness variations, and mixtures of materials, to name a few, with adjustable initial wave lengths and amplitudes. Figure 4 shows a typical double Al-target in which the top (irradiated) foil has a 300 μm ripple.

In these experiments, the incident beam is relatively uniform (± 30%), with intensity distribution shown in the top of Figure 3b, to provide as uniform an ablation pressure as presently possible. The velocity uniformity of the resulting accelerated target, $\delta v/v \lesssim \pm 7\%$, is shown for reference. When an identical thickness rippled foil is accelerated under the same conditions, a 20% velocity perturbation is observed with about the imposed wavelength implying, a spatial amplitude about 28 times that present initially. Similarly, targets with a 1/2 μm thickness variation also yield an enhanced perturbation having the imposed wavelength. A hydrodynamic model describing effects such as these is found in reference 32. However, a simple kinematic model can also account for most of the observed perturbation developed during the acceleration of the targets with thickness (areal density) variation. Under constant pressure the thicker portions of the target have a lower acceleration and, hence, lower final velocities than the thinner region. The observed spatial amplitude is within a factor of two of this estimate. Targets with no mass variation but ripples also exhibit amplitude modulation enhanced over those originally present. The ratio of ripple amplitude to wavelength was small initially (10^{-2}) and therefore kinematics due to a mass variation cannot explain the results. Other kinematic type effects such as those resulting from refraction of the incident light in rippled underdense plasma may be capable of causing the enhanced perturbation. Interestingly, both a constant acceleration Rayleigh-Taylor model with a growth rate $\gamma t = \sqrt{2kL}$ and a Richtmeyer shock Rayleigh-Taylor model, where $\delta x = kx_o L$, predict $\delta x/x_o$ of 10 to 20. Experiments and theory designed to provide definitive identification of the mechanisms are underway.

An important distinction between nonuniformities resulting from imperfections on the target rather than the beam is that thermal conduction cannot significantly help smooth out long scalelength nonuniformities due to target structure since the temperature is very low at the ablation surface and thermal conduction is poor. Thus, it is imperative to identify and control the structural mechanisms involved in nonuniform target acceleration.

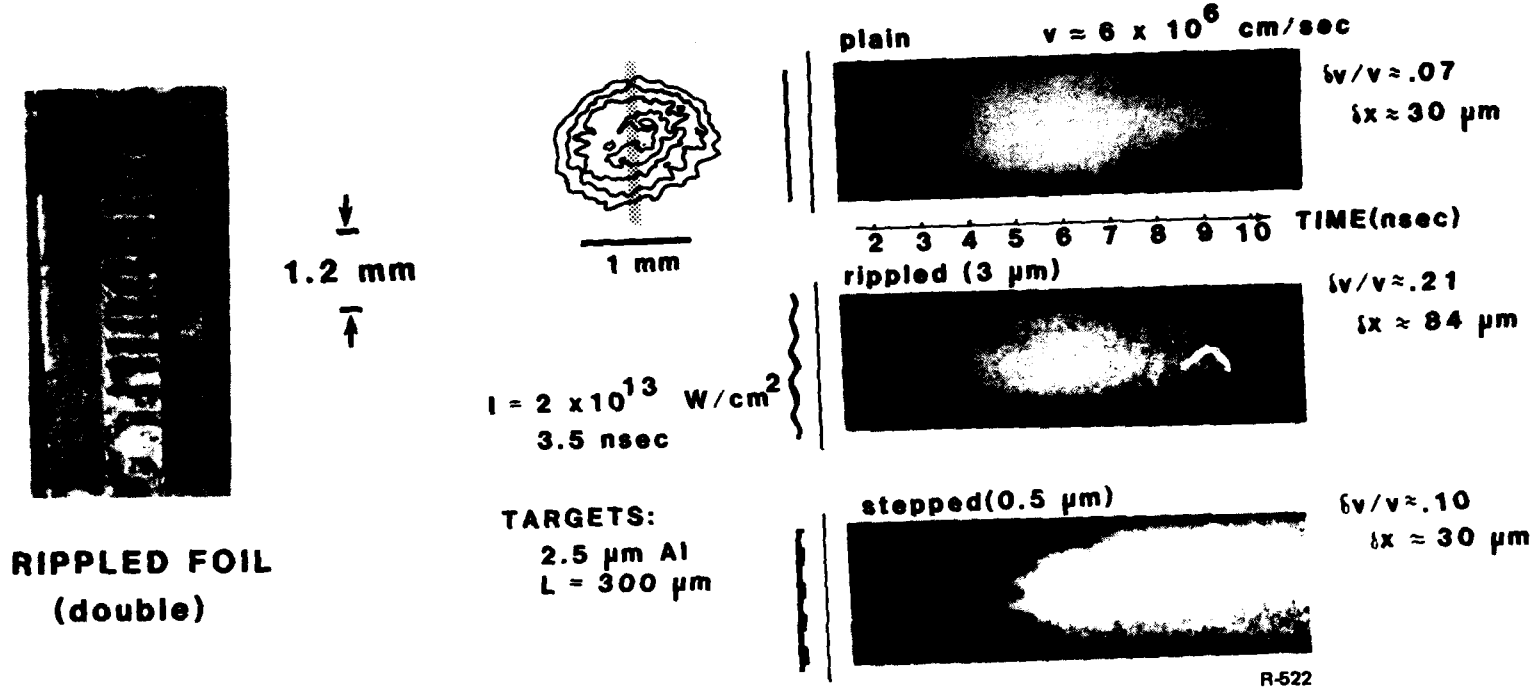

Fig. 4 — Nonuniformities due to ablative acceleration of nonuniform Al targets (left), a sample rippled foil, (center), the focal spot distribution and experimental conditions, and (right) double-target streak photograph of target accelerations with a plain target (top), a rippled target (center) and a stepped target (bottom). Laser pulse duration was 3.5 nsec FWHM and was focused to approximately 10^{13} W/cm^2.

CONCLUSIONS AND SUMMARY

Thus far we have shown that dense targets can be ablatively accelerated to high speed. That is, targets have been accelerated to speeds of 160 km/sec at mid x 10^{13} W/cm^2 which are, simultaneously, uniform to $\pm$ 7%, and on a relatively low isentrope T < 10 eV. Coupling efficiency into kinetic energy as high as 16% has been observed. Moreover, nonuniformities present in the incident beam are more effectively damped out with increasing irradiance and perturbation wave number. The final conditions found in our experiments at NRL, shown in Table I, are within a factor of a few of those required. In a recent experiment done in collaboration with LLNL on the SHIVA laser it was verified that the acceleration uniformity improved further at 10^{14} W/cm^2, to better than $\pm$ 3.5% and the laser coupling physics remained benign.[17]

Some additional factors that may be important but are not addressed here include: the effects of spherical geometry, wavelength scaling of the interaction physics and symmetrizing mechanisms and the effect of broad bandwidth laser illumination.

A spherical geometry effect that may be important is a possible reduction of hydrodynamic efficiency by up to a factor of 3 from the corresponding planar case. The actual magnitude of this effect remains to be tested. There are also symmetry considerations that will be a function of spherical geometry. If the distance between laser light absorption and ablation decreases, due to the higher density gradient in three-dimensional versus planar expansion, then the uniformity requirements increase for spherical geometry. Finally, effects of internal pressure of any material within the shell or the stability of the inner surface during the compression phases are not addressed in planar geometry, but indeed may present important symmetry issues.

The scaling of the distance between absorption and ablation surfaces with laser wavelength has also not yet been explored experimentally. However, this "cloudy day" effect is generally thought to scale like $d \propto I^{0.7} \lambda^{2.7}$ from both analytic theory and numerical hydrodynamic code calculations. Thus, if additional symmetrization is required to reduce irradiation nonuniformities, a slightly longer laser wavelength may be desirable. One possibility is the HF chemical system which has broad bandwidth between 2.5 and 3 μm, and is also potentially efficient. It remains to be determined if broad bandwidth increases the threshold for deleterious plasma effects sufficiently for the HF laser to be useful as a driver for target acceleration.

Another important set of questions to be answered, hopefully in the near future, relate to the scaling of the interaction physics and nonuniformity smoothing to larger systems, of several millimeter dimensions. In addition, the roles of target structural nonuniformity and hydrodynamic instability need further exploration.

We thank M. Fink, N. Nocerino, B. Sands, and E. Turbyfill for their technical contributions, and E. Campbell, D. Phillion, R. Price and M. Rosen of LLNL for their participation on the joint SHIVA experiment.

REFERENCES

1. S.E. Bodner, J. Fusion Energy 1 (1981) 221.

2. B.H. Ripin, R. Decoste, S.P. Obenschain, S.E. Bodner, E.A. McLean, F.C. Young, R.R. Whitlock, C.M. Armstrong, J. Grun, J.A. Stamper, S.H. Gold, D.J. Nagel, R.H. Lehmberg, and J.M. McMahon, NRL Memo Report #3890 (1978); Phys. Fluids 23 (1980) 1012 and 24 (1981) 990.

3. R. Decoste, S.E. Bodner, B.H. Ripin, E.A. McLean, S.P. Obenschain, and C.M. Armstrong, Phys. Rev. Lett. 42 (1979) 1673.

4. B.H. Ripin, R.R. Whitlock, F.C. Young, S.P. Obenschain, E.A. McLean, and R. Decoste, Phys. Rev. Lett. 43 (1979) 350.

5. E.A. McLean, S.H. Gold, J.A. Stamper, R.R. Whitlock, H.R. Griem, S.P. Obenschain, B.H. Ripin, S.E. Bodner, M.J. Herbst, S.J. Gitomer, and M.K. Matzen, Phys. Rev. Lett. 45 (1980) 1246.

6. J. Grun, R. Decoste, B.H. Ripin, and J. Gardner, Appl. Phys. Lett. 39 (1981) 545.

7. J. Grun, S.P. Obenschain, B.H. Ripin, R.R. Whitlock, E.A. McLean, J. Gardner, M.J. Herbst, and J.A. Stamper, NRL Memo Report #4747 (1982); accepted for publication in Phys. Fluids.

8. S.P. Obenschain, R.H. Lehmberg, and B.H. Ripin, Appl. Phys. Lett. 37 (1980) 903.

9. S.P. Obenschain, J. Grun, B.H. Ripin, and E.A. McLean, Phys. Rev. Lett. 46 (1981) 1402.

10. M.J. Herbst, R.R. Whitlock, and F.C. Young, Phys. Rev. Lett. 47 (1981) 91; Phys. Rev. Lett. 47 (1981) 1568.

11. B.H. Ripin, S.E. Bodner, S.H. Gold, R.H. Lehmberg, E.A. McLean, J.M. McMahon, S.P. Obenschain, J.A. Stamper, R.R. Whitlock, F.C. Young, H.R. Griem, J. Grun, and M.J. Herbst, NRL Memo #4212 (1980).

12. B.H. Ripin, S.E. Bodner, J. Grun, M.J. Herbst, E.A. McLean, J.M. McMahon, S.P. Obenshcain, J.A. Stamper, R.R. Whitlock, and F.C. Young, Ultraviolet and VUV Systems, Proc. SPIE 279 (1981) 46.

13. J.M. McMahon et al., IEEE J. Quant. Elec. QE17 (1981) 1629.

14. M.J. Herbst and J. Grun, Phys. Fluids 24 (1981) 1917.

15. M.J. Herbst, R.R. Whitlock, J.A. Stamper, R.H. Lehmberg, F.C. Young, J. Grun, and B.H. Ripin, Proc. of Symmetry Aspects of Inertial Fusion Implosions, NRL Report (1981).

16. M.J. Herbst et al., NRL Memo #4893 (1982).

17. S.P. Obenschain, R.R. Whitlock, E.A. McLean, B.H. Ripin, R.H. Price, D. Phillion, E.M. Campbell, and M.D. Rosen, to be published.

18. E.M. Campbell, et al., Proc. of IEEE Intl. Conf. on Plasma Science, IEEE Cat. #82CH1770-7 (1982) 55; to be published.

19. J.A. Stamper, E.A. McLean et al., NRL Memo # (1982).

20. S.P. Obenschain, J.A. Stamper, E.A. McLean, M.J. Herbst, S.E. Bodner, R.H. Lehmberg, J.M. McMahon, J. Grun, R.R. Whitlock, and B.H. Ripin, Proc. of Symmetry Aspects of Inertial Fusion Implosions, NRL Report (1981).

21. M.J. Herbst, J.A. Stamper, R.R. Whitlock, R.H. Lehmberg, and B.H. Ripin, Phys. Rev. Lett. 46 (1981) 328.

22. J.A. Stamper, E.A. McLean, and B.H. Ripin, Phys. Rev. Lett. 40 (1978) 1177.

23. S.P. Obenschain, E.A. McLean, and S.H. Gold, Rev. Sci. Instr. 51 (1980) 1661.

24. R.R. Whitlock, S.P. Obenschain, J.M. McMahon, and B.H. Ripin, Proc. of Symmetry Aspects of Inertial Fusion Implosions, NRL Report (1981); to be published in Appl. Phys. Lett.

25. M.H. Emery, J.H. Gardner, J.P. Boris, and J.H. Orens, NRL Memo #4500 (1981).

26. M.H. Emery and J.H. Gardner, Phys. Rev. Lett. 48 (1982) 677.

27. W.M. Manheimer, D.G. Colombant, and J.H. Gardner; submitted to Phys. of Fluids.

28. J.H. Gardner and S.E. Bodner, Phys. Rev. Lett. 47 (1981) 1137.

29. B.H. Ripin, E.A. McLean, and J.A. Stamper, NRL Memo Report #4811 (1982); accepted for publication in Phys. Fluids.

30. B.H. Ripin, et al., Bull. Am. Phys. Soc. 25 (1980) 946.

31. J. Grun, et al., presented at 12th Ann. Anomalous Absorption Conference, May (1982).

32. M. Emery, et al., IAEA-CN-41/W-9 (1982).